Simulation methodologies of engine noise shielding by wings within conceptual aircraft design

Vieira, Ana; Koch, Marc; Bertsch, Lothar; Snellen, Mirjam; Simons, Dick G.

DOI
10.2514/1.C035847

Publication date
2020

Document Version
Final published version

Published in
Journal of Aircraft

Citation (APA)
Vieira, A., Koch, M., Bertsch, L., Snellen, M., & Simons, D. G. (2020). Simulation methodologies of engine noise shielding by wings within conceptual aircraft design. *Journal of Aircraft*, *57*(6), 1202-1211. https://doi.org/10.2514/1.C035847

JOURNAL OF AIRCRAFT
Vol. 57, No. 6, November–December 2020

Simulation Methodologies of Engine Noise Shielding by Wings Within Conceptual Aircraft Design

Ana Vieira*
Delft University of Technology, 2629 HS Delft, The Netherlands
Marc Koch† and Lothar Bertsch‡
DLR, German Aerospace Center, 37073 Göttingen, Germany
and
Mirjam Snellen§ and Dick G. Simons¶
Delft University of Technology, 2629 HS Delft, The Netherlands

https://doi.org/10.2514/1.C035847

The pursuit of greener aviation led to the investigation of new aircraft concepts. Disruptive aircraft configurations show great potential in reducing the ground noise impact, but extensive research is required before they can be manufactured. Tube-and-wing aircraft with over-the-wing engines, benefiting from noise shielding, are a more feasible option for midterm noise reduction targets. This work explores a low-noise version of the B747-400 considering over-the-wing engines, and a multidisciplinary procedure is used to calculate the aircraft and engine performance, the flight procedure, and the noise impact. Engine positions are found providing maximum engine noise shielding, reflected in a decrease in the sound exposure level (SEL) contours. These contours are calculated considering the wing leading edge as both a sharp and a curved edge. This work investigates whether a sharp leading-edge approximation is acceptable for first estimates of the optimal engines position and corresponding noise reduction values. From the results it is found that the maximum decrease in the SEL obtained for the modified aircraft is 2 dB considering a sharp leading edge and 1.5 dB for a curved leading edge, for departure. For approach, the SEL contours do not show significant differences for the sharp and curved leading edge, with maximum noise reduction values of 3.5 dB for both cases.

Nomenclature

A_{SEL}	=	isocontour area of sound exposure level, m^2
A_{wing}	=	wing area, m^2
$E_{\mathrm{cruise,beg}}$	=	glide ratio begin cruise flying design mission
g_i	=	weighting according to the time slot of the flight event i
h	=	aircraft altitude, m
L_{Aeq}	=	A-weighted equivalent continuous sound level, dBA
L_p	=	overall sound pressure level, dB
M_{cruise}	=	design cruise Mach number
N	=	number of flight events
N_1	=	rotational speed of the fan relative to the maximum value, %
SEL	=	sound exposure level (synonym for $L_{p,\mathrm{AE}}$), dB
T	=	observation time, s
TAS	=	true air speed, m/s
v	=	aircraft velocity, m/s
x_{fdc}	=	distance in the length of the aircraft relative to the noise, m
γ_1	=	descent angle, °
θ	=	polar angle, °
λ_F	=	wing aspect ratio
Λ	=	wing sweep, °

Subscripts

cb	=	cutback
eow	=	engines over the wings
i	=	flight event
rr	=	reduced range

I. Introduction

ACCORDING to the International Civil Aviation Organization's (ICAO's) balanced approach, several technical and nontechnical measures are available to effectively reduce aircraft noise [1]. The balanced approach is directly derived from a time-averaged, weighted level L_{Aeq}:

$$L_{\mathrm{Aeq}} = 10 \cdot \log 10\left(\frac{1}{T}\sum_{i=1}^{N} g_i \cdot 10^{\mathrm{SEL}_i/10}\right) \tag{1}$$

Equation (1) describes the L_{Aeq} at a certain observer location and is affected by nontechnical factors (number of flight events N and weighting according to time of flight event g_i) and technical factors (sound exposure level for each flyover event SEL_i). T is the observation time. L_{Aeq} is a widely accepted and applied metric to assess aircraft noise exposure around major airports; e.g., contour areas of this metric are applied to define noise protection zones [2] in Germany. To reduce the noise exposure for communities, the L_{Aeq} has to be reduced as much as possible [3]. This contribution investigates a reduction of noise impact on the ground by shielding of engine noise by the airframe and an adjustment of the flight procedure, resulting in a reduction of SEL along approach and departure over a wide area. For this study, the focus is on noise shielding of the engine fan as one of the most promising modifications [4]. Different simulation approaches and aircraft geometry and noise source approximations

Received 14 January 2020; revision received 27 May 2020; accepted for publication 4 June 2020; published online 17 July 2020.

*Ph.D. Candidate, Aircraft Noise and Climate Effects Section, Faculty of Aerospace Engineering; a.e.alvesvieira@tudelft.nl.
†Ph.D. Candidate, Institute of Aerodynamics and Flow Technology; marc.koch@dlr.de.
‡Researcher, Institute of Aerodynamics and Flow Technology, Bunsenstr. 10; lothar.bertsch@dlr.de.
§Associate Professor, Aircraft Noise and Climate Effects Section, Faculty of Aerospace Engineering; m.snellen@tudelft.nl.
¶Full Professor, Aircraft Noise and Climate Effects Section, Faculty of Aerospace Engineering; d.g.simons@tudelft.nl.

are available to assess this shielding [5–7]. In this research work predictions are made considering a sharp and a curved leading edge. This can have a direct impact on the predictions, the drawn conclusions, and consequently on the selected location of the engines. The focus of this study lies on the comparison of the two simulation approaches and its impact on a low-noise aircraft design process.

The selected application is a conventional long-range tube-and-wing aircraft, similar to a B747-400. Other ideas of noise shielding concepts, e.g., the vehicle *fanex* [5] or *V*-2 [4], differ significantly from conventional aircraft.

To evaluate the different simulation approaches applied to noise shielding for multiple engines under the constraint of low computational costs, a new noise shielding tool developed by the Technical University of Delft (TU Delft) [8,9] is applied here. It is specifically focused for application in low-noise aircraft design processes. It provides delta levels that can directly be fed into the overall aircraft noise prediction. For the selected application, additional modifications to the existing framework [10,11], i.e., aircraft design and overall aircraft noise prediction, were required in order to account for the multiple engines and their installation above larger shielding surfaces.

This introductory section is followed by Sec. II, which describes the selected methodology, including noise shielding, aircraft and engine design, flight simulation, and overall noise prediction. Section III presents the experimental procedures used to validate the methods used in this work. Section IV analyzes the selected application case and introduces the long-range transport reference aircraft and its low-noise retrofit version. Finally, Sec. V summarizes and discusses the obtained results.

II. Methodology

Prerequisite of any modification to the aircraft is a clear understanding and comprehensive simulation of the possible implications on other disciplines such as the flight performance. Advantageous shielding locations for the engines could negatively influence the flight performance; e.g., increased drag or weight would result in higher engine thrust requirements, which counteracts any anticipated noise reduction. Therefore, the overall noise assessment of any new aircraft concept has to focus on the ground noise impact based on a detailed aircraft design and flight simulation, i.e., taking into consideration modifications to the vehicle design and the corresponding flight performance. For this task, an existing simulation framework of the German Aerospace Center (DLR) and the Technical University of Braunschweig (TU Braunschweig) [4,12] is applied. This framework can be used to investigate and optimize the aircraft ground noise impact along simulated approach and departure flight procedures.

The levels of the different noise sources can strongly vary; e.g., airframe noise contribution can even dominate the overall aircraft noise under certain operating conditions during approach. These effects are accounted for when investigating the potential noise decrease due to shielding. Furthermore, distances between source and receiver that are typically associated with community noise annoyance lie in the order of 500–2000 m. For such distances, the frequency-dependent atmospheric propagation effects have a significant impact on the received noise levels on the ground. Consequently, the noise shielding, which is highly frequency dependent, has to be evaluated for varying flight altitudes along typical approach and departure flights.

The selected simulation framework for this study addresses all of the before mentioned problems. The framework considers the aircraft and engine design [12,13], detailed approach and departure flight simulation [14], noise shielding assessment [8,9], and finally the overall aircraft noise prediction [4].

A. Aircraft and Engine Design

The simulation process is based on the Preliminary Aircraft Design and Optimization (PrADO) tool developed by TU Braunschweig [12]. PrADO calculates the aircraft geometry, component and total masses, and aerodynamic and engine data. Because of PrADO's modular structure, specific modules can be replaced by external numerical or experimental data. For this work, PrADO uses an external engine performance map, calculated with Gas Turbine Laboratory (GTlab) by the Institute of Propulsion Technology, DRL Cologne [13]. GTlab is a component-based simulation framework for turbo engine and gas turbine simulations. It calculates the thermodynamic cycle for both design and off-design conditions. Additionally to stationary operations, also basic transient operations can be simulated. Main geometrical details as required for a noise assessment are also generated [4]. PrADO processes the external GTlab engine performance deck to enable an overall design synthesis.

B. Flight Simulation and Low-Noise Trajectory Calculation

The Flightpaths for Noise Analysis (FlipNA) tool is used to calculate tailored and realistic trajectories [15], using the output of PrADO (aerodynamics and vehicle mass) and GTlab (engine performance). A low-noise approach trajectory can be obtained by reducing both the engine rotational speed and aircraft airspeed, which are directly correlated with noise generation. Additionally, the high lift devices and the landing gear should be deployed as late as possible to avoid excessive airframe noise.

The low-noise takeoff trajectory considers full engine power, takeoff performed with $N_1 = 105\%$, followed by cutback where engine speed is reduced to $N_1 = 100\%$ (equal to 3280 rpm). Acceleration and climb is performed with $N_1 = 100\%$. All flight profiles are simplified by neglecting the presence of wind.

C. Overall Noise Assessment

The noise assessment is determined using the Parametric Aircraft Noise Analysis Module (PANAM). This parametric noise prediction model assesses both the aircraft noise emission and the impact on the ground. To perform a noise assessment with PANAM, the following input data are required: the aircraft geometry, trajectory, shielding capability, engine deck, and observer positions. The trajectory input for PANAM describes the aircraft position and orientation, and the settings of the high lift devices, landing gear, and engines.

The shielding values are calculated for the fan noise using the method described in Sec. II.D, and not applying the standard DLR tool as documented in previous work [16]. The TU Delft method specifically enables the study of the two simulation approaches, i.e., a wing representation considering a sharp leading edge versus a curved leading edge.

In the simulation process, all engines are considered to run at the same operating point and consequently present equal noise emission. The noise shielding factors are finally applied to the fan noise predictions of PANAM. Fan noise is divided into two noise sources, positioned at the inlet and nozzle of the engine. This approach can be more accurate than considering a single noise source centered at the fan disk center [17].

Installation effects, such as reflection of jet noise on the wing, are not included in the semi-empirical prediction models used in this work. Computationally expensive high-fidelity models are usually used to determine installation effects [18]. However, including high-fidelity methods in the optimization of the engine location of the low-noise version of the B747-400 is not feasible within the conceptual design phase, as it would drastically increase the computational time.

Standard noise metrics such as the integral metric SEL are used to assess the noise impact. An iterative process is used to find the aircraft final design, approach, and takeoff trajectories, as illustrated in Fig. 1.

D. Noise Shielding

The noise shielding values are used to select the engine position and therefore should be accurately estimated. Because of the large dimension of the wingspan in relation to the airfoil thickness, the wing is first approximated as a flat plate within this study. This is an acceptable approximation when the radius of the curvature of the

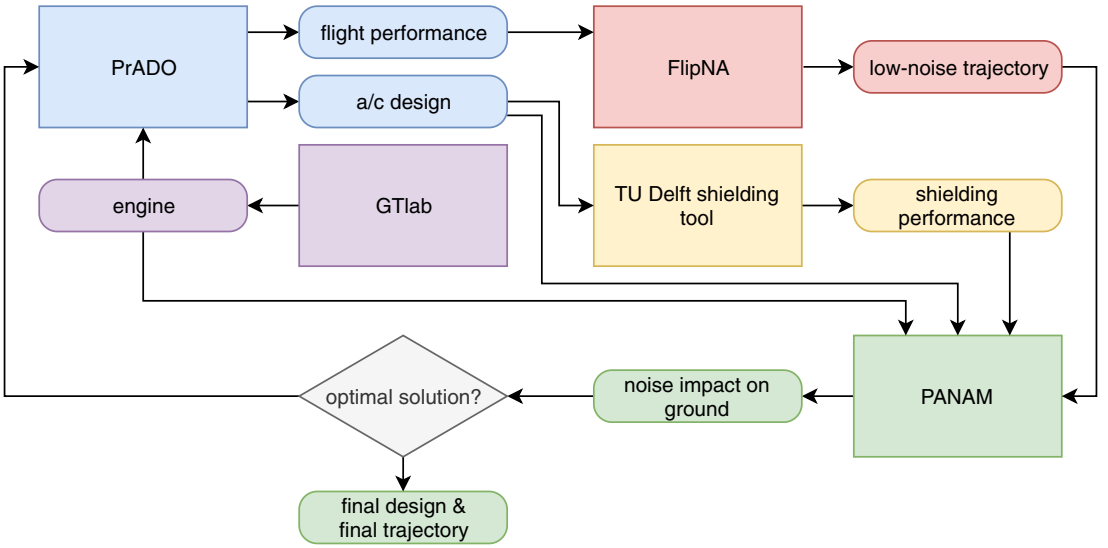

Fig. 1 Overall simulation process.

leading edge is small compared with the wavelength, but as the frequency increases, the effect of the curvature of the wing leading edge affects the noise shielding values [19].

In the presence of an obstacle, the incident acoustic pressure field is modified, and the diffracted field is composed by edge-diffracted and creeping rays. The edge-diffracted rays are originated when the ray is incident on a sharp edge. When the surface has a curvature, the ray lies partially on that surface, and it is denominated a creeping ray. The behavior of the two types of rays is illustrated in Fig. 2. The field diffracted at the curve decreases exponentially with the wavelength, and therefore it is weaker than the field diffracted by a sharp edge [19]. These findings led to the present study. The effect of the two approaches is consequently evaluated on an aircraft system level, i.e., the effect on the ground noise impact.

The method used to predict noise shielding in this work is based on the Kirchhoff integral theory [20] and the modified theory of physical optics (MTPO) [21]. For a detailed description of the method used to calculate the edge-diffracted and creeping rays, the reader is referred to [8,9]. This method calculates the diffracted field by an aperture of the same size and shape as the obstacle. The diffracted field is then used to determine the scattered field by the obstacle using Babinet's principle [22]. A perturbation of the incident field, such as the introduction of an obstacle, modifies it and it is then denominated scattered field. The value of noise shielding at a receiver position is determined by the difference between the resultant scattered field and the undisturbed incident field.

In this research, the fan noise was modeled as two monopoles, at the inlet and nozzle of the engine. The required inputs are the aircraft geometry and the position of the noise sources. The noise shielding values are calculated for a half-hemisphere of 100 m radius centered at the noise source, with a discretization of 2°. Therefore, noise shielding values are available for any azimuthal and polar position of the observers on ground relative to the noise source and can be directly subtracted from the fan noise in PANAM.

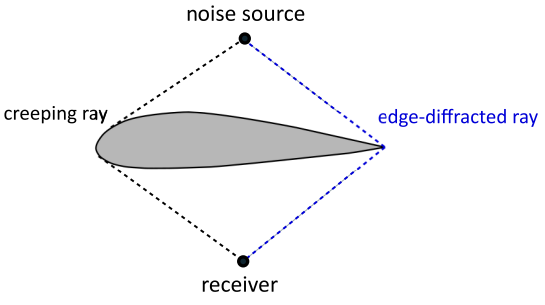

Fig. 2 Edge-diffracted and creeping rays in a wing section.

III. Experimental Validation of the Methodology

This section provides a brief description of the data used to validate the computational methods used in this research. PrADO has been validated in several research works for conventional aircraft using experimental data provided by manufacturers [12,23,24]. GTlab results were compared with the IAE-V2527 engine, and calibrated with experimental data [25]. The development and validation of FlipNA can be found in reference [14]. The results of PANAM were extensively compared with experimental data [4]. These tools are parametric and semi-empirical, and hence can be applied to other conventional aircraft than the validations cases. The reliability of these tools can be strongly reduced if applied to significantly different designs, e.g., vehicles with fully embedded and distributed propulsion.

The TU Delft noise shielding tool was recently developed, and both flyover and wind tunnel measurements were used for the comparison with predictions. The wind tunnel experiment consisted of an omni-directional source shielded by a scale model wing. The reader is referred to [9] for a complete description of the experiment. The noise shielding values measured for the wing were compared with the values found for a sharp edge plate of the same dimension as the wing. It was verified that the noise shielding values were different for the two shielding objects, for the same observer and source positions. This shows that the curvature of the leading edge affects the noise shielding. The predictions showed a good agreement with the measurements for both the wing and the flat plate.

The experimental validation of models for noise shielding predictions for an aircraft is a difficult task, not only due to the complex nature of engine noise, detailed geometry of the aircraft, and atmospheric effects, but also because few commercial models have the engines located over the wings. Flyovers of different aircraft models were recorded during an experimental campaign in Schiphol airport, in Amsterdam, using a microphone array positioned in a landing track. Those measurements included a significant amount of flyovers of the Fokker 70 (F70), which has over-the-wing engines. A detailed description of the experiments and comparison with prediction can be found in [8].

Here, for illustrative purposes we show Fig. 3, presenting the overall sound pressure level (L_p) measured for two of the flyovers recorded (black line), the L_p predicted when noise shielding is not considered (blue line), and the predictions of L_p considering shielding with a sharp leading edge (green line) and a curved leading edge

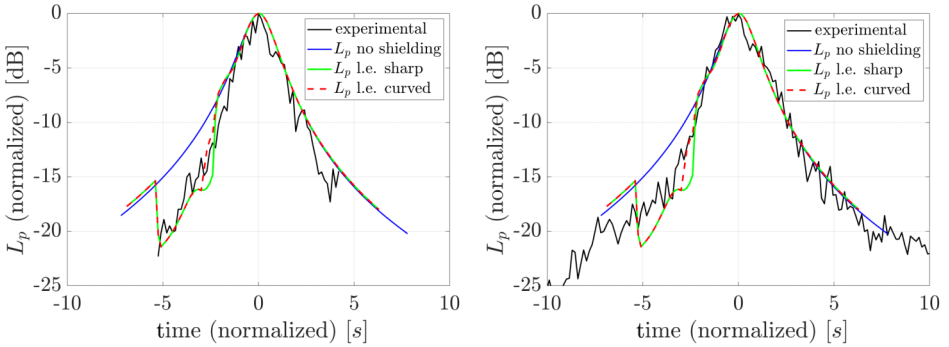

Fig. 3 Measured (black line) and predicted (colour lines) values of L_p during two F70 flyovers for an observer aligned with the aircraft approach trajectory. Here l.e. stands for leading edge.

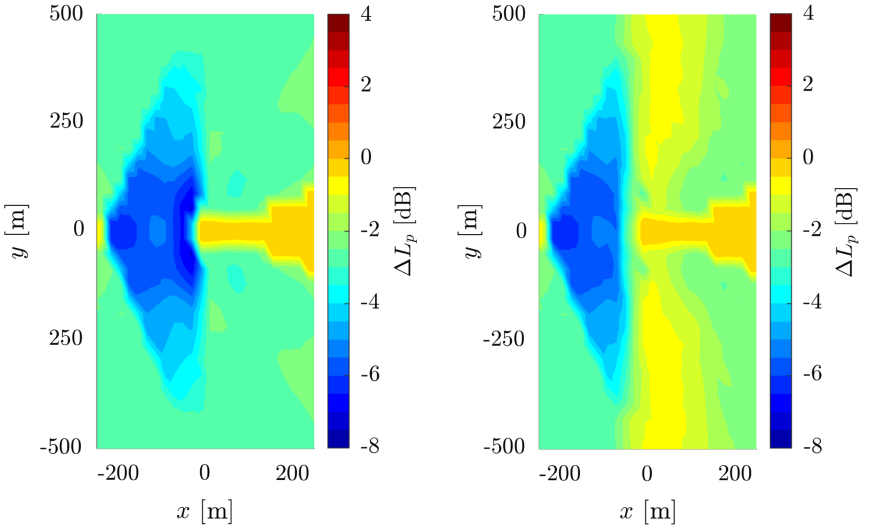

Fig. 4 Predictions of noise shielding on ground considering the leading edge sharp (left) and with a curvature (right).

(dashed red line). All L_p values are normalized by their maximum value.

There is a clear region, between 2 and 5 s before overhead, in which the experimental L_p curve does not correspond to the prediction with no shielding (blue line). This is associated to noise shielding, which is supported by the predictions. The predictions of noise shielding with the sharp and curved leading edge are similar and in agreement with the experimental curve. Other flyovers, not presented in this work, showed similar results. The experimental results present some variability, and therefore it is not possible to determine the exact difference between experimental and predicted noise shielding values.

The effect of a curved leading edge does not seem very significant in Fig. 3, but this represents just one observer position aligned with the approach trajectory. The differences in noise shielding between a sharp and curved leading edge are more evident for other observer positions, as one can see comparing the plots of Fig. 4. These plots represent the values of noise shielding on ground, with the center of the aircraft located at $x = 200$ m at a height of 70 m. These results indicate that not considering the curvature of the leading edge might lead to differences in the predicted noise impact.

IV. Low-Noise Version of the B747-400

In this section the framework of Fig. 1 is applied to design a low-noise version of the B747-400. The B747-400 and its low-noise version, here denominated $B744_{\text{eow}}$ (B747-400 engines over the wing), are shown in Fig. 5. The noise impact on the ground is minimized by finding an optimal position for the engines in terms of noise shielding.

The reference aircraft and its low-noise version are described in Sec. IV.A, and the low-noise approach and departure trajectories are

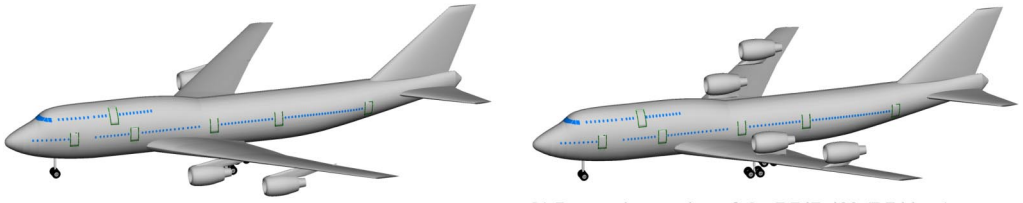

a) B747-400 reference vehicle **b) Low-noise version of the B747-400 ($B744_{\text{eow}}$)**

Fig. 5 B747-400 aircraft and $B744_{\text{eow}}$ variant for high shielding.

presented in Sec. IV.B. The optimal position of the inboard and outboard engines is investigated in Sec. IV.C together with the assessment of the noise impact of the final design of the $B744_{eow}$, during landing and approach. In Sec. IV.C the results are presented considering both a sharp and a curved leading edge.

A. Aircraft and Engine Description

Moving the engines to the top of the wings increases the drag due to stronger wave drag. This leads to more fuel consumption and therefore to an unacceptable maximum takeoff weight (MTOW). Consequently, the range of the $B744_{eow}$ had to be reduced to 8100 km, whereas the original B747-400 has a design range of 10,600 km.

However, with this modification of range, the noise impact of the two models is not comparable. Another variation of the B747-400, denominated $B744_{rr}$ (reduced range), is calculated with PrADO for the comparison. The payload range chart of the $B744_{eow}$ and the $B744_{rr}$ is presented in Fig. 6. For validation purposes the payload range chart predicted with PrADO is compared with Boeing's official data of the B747-400 in Appendix A.

Figure 6 shows that, even with the range modification, the payload range chart of the $B744_{rr}$ and the $B744_{eow}$ is not exactly the same. The cruise speed was decreased from Mach 0.85 for the $B744_{rr}$ to 0.7 for the $B744_{eow}$ due to the drag increase. Even with a lower cruise speed, the increase of drag in the $B744_{eow}$ leads to 18% more fuel consumption compared with the $B744_{rr}$. Appendix B summarizes the differences between the $B744_{rr}$ and the $B744_{eow}$ designs. The geometry of the $B744_{rr}$ is the same as the original B747-400, but the wing

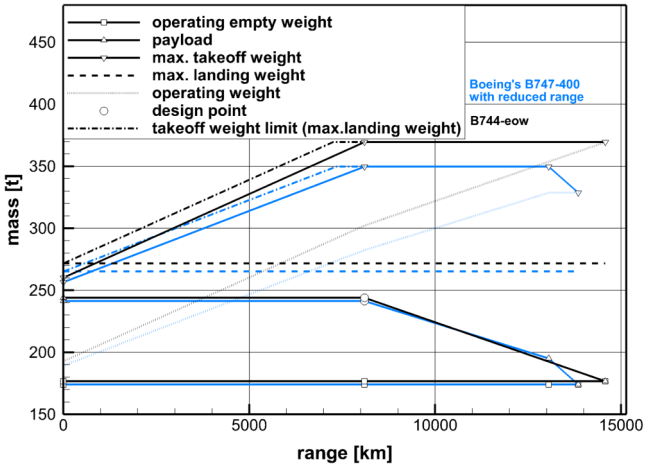

Fig. 6 Payload range chart for the $B744_{rr}$ with a reduced range as a new reference vehicle and the low-noise variant, $B744_{eow}$.

geometry of the $B744_{eow}$ presents some small modifications (wing area and aspect ratio) due to changes in the aerodynamics.

The four power plants were calculated with GTlab, described in Sec. II.A, and were based on the CF6-80 engine. The 4.27 m long engine is equipped with 38 fan blades, providing a 273 kN takeoff thrust. The inlet and aft engine noise sources are considered individually, and respective shielding factors are predicted at the inlet and nozzle [17].

B. Trajectories and Noise Emission of the Reference Aircraft

The determined low-noise approach and departure trajectories for the $B744_{rr}$ are presented in Figs. 7a and 7b, respectively. The trajectories were determined following the design rules described in Sec. II.B.

In the low-noise approach trajectory, in Fig. 7a, the first descent section with a descent angle of $\gamma_1 \approx -2.7°$ (identified as segment 1 in the plot) has the engine speed set to idle and the aircraft maintains 1.3 times the stall speed. The high lift devices are deployed at point 2 to avoid acceleration and the aircraft finally descends with $-3°$. In segment 3 the landing gear is deployed and the flaps are fully set. Once the stabilization point is reached at 300 m, the velocity, trajectory slope, and angle of attack are kept constant. The thrust is increased to compensate the drag originated by the high lift devices and the landing gear.

The departure is conducted with full thrust up to the cutback point, identified as 4 in Fig. 7b, and continued with a cutback rotational speed of $N_{1,cb} = 100\%$. Once the airspeed reaches 130 m/s, the aircraft gains altitude on segment 5 up to cruise altitude.

Representative phases along the approach and departure trajectories are selected to show the different noise sources and their importance to the total noise emission. Figure 8a shows the noise emission of the $B744_{rr}$ for approach at 15 km before the approach threshold ($h = 800$ m, $v = 103$ m/s, engine in idle at $N_1 = 35\%$, flaps set to 20°), and Fig. 8b the noise emission for departure, 12.5 km after brake release ($h = 820$ m and $v = 133$ m/s, $N_1 = 100\%$, high lift devices configuration is clean).

For the approach situation selected, airframe noise is the dominant noise source for all polar directions. Fan forward and fan aft noise are, respectively, 17 and 10 dB below airframe noise. In contrast, during departure, fan noise is dominant, followed by jet noise. Additionally, airframe noise has a negligible contribution. Figure 8 indicates that noise emission can be greatly reduced during departure by shielding of fan noise. For approach, however, the shielding of fan noise is expected to have little impact on noise emission.

C. Overall Noise Assessment of the Low-Noise Aircraft

The aim of this section is to assess the ground noise impact for the $B744_{rr}$ and the $B744_{eow}$, along approach and departure. First, the

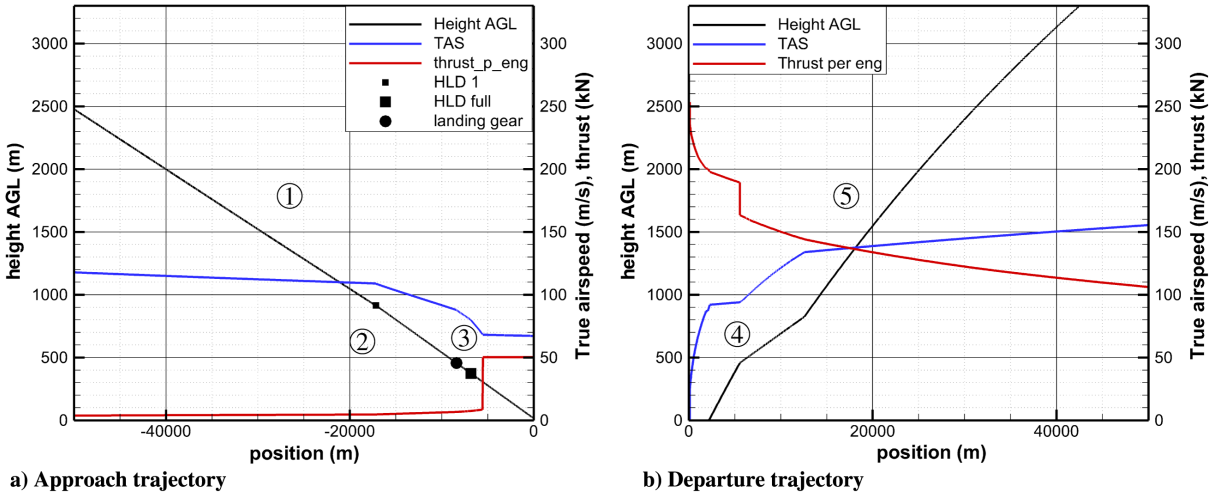

a) Approach trajectory **b) Departure trajectory**

Fig. 7 Approach and departure trajectories for the $B744_{rr}$.

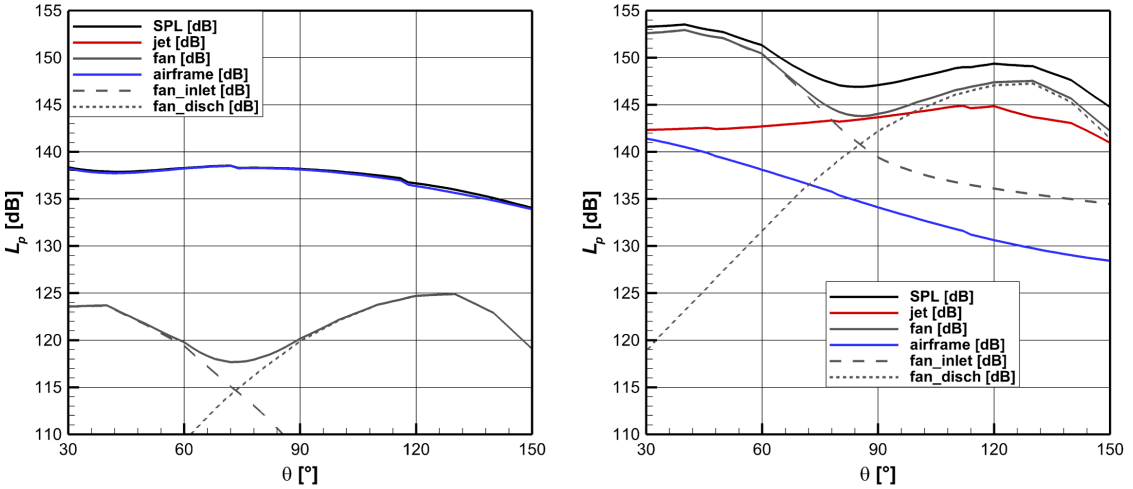

a) Emission for selected approach situation **b) Emission for selected departure situation**

Fig. 8 Overall sound level for the $B744_{rr}$ for the approach and departure conditions selected.

positions of the inboard and outboard engine of the $B744_{eow}$ are determined to achieve maximum noise shielding. Then, the noise emission is evaluated for one operating point along the approach and departure for the $B744_{rr}$ and compared with the corresponding case for the $B744_{eow}$. Finally, the noise impact on ground is determined and compared for the two aircraft, according to the different simulation methods to assess noise shielding, i.e., the influence of considering the creeping rays.

1. *Selection of the Optimal Engine Position*

The engine positions subjected to maximum shielding are determined individually for the inboard and outboard engines. The engines are moved downstream on the wing, and the 80 dB SEL contour area is assessed for each position x_{fdc} (position of the engine relative to the nose of the aircraft). This is the criterion to determine the engine position with maximum shielding for the inboard and outboard engines.

Figure 9 shows the contour area of 80 dB SEL for different positions of the inboard and outboard engines. Engine locations have been investigated in discrete steps of 0.5 m. The orange line shows the 80 dB SEL contour area of the $B744_{rr}$. Figures 9a and 9b were found considering the leading edge as sharp in the noise shielding calculations. Figures 9c and 9d considered a curved leading edge.

Figures 9a and 9c indicate that the most promising position of the inboard engines is 34 m relative to the aircraft nose for a sharp leading edge, and 33.5 m for a curved leading edge, i.e., one discrete step size. For the outboard engine, the optimal position is 42 m for a sharp leading edge and 40 m for a curved leading edge (difference of 4 discrete steps). An SEL area change of 20% can be associated with a source noise reduction of approximately 1 dBA [26].

Figure 10 shows the optimal inboard and outboard engines position in the chord, for both cases of a sharp and a curved leading edge. The dimensions of the airfoil section are realistic, as well as the positions of the fan inlet and exhaust in the chord direction. The fan disk center is represented by a black cross and the fan inlet and exhaust by dots (blue for the position found considering a sharp leading edge, and black for a curved leading edge). The distance of the engine relative to the surface of the wing changes along the chord direction, which is also accounted for in this scheme.

The more the engines are centered on the wing chord, the larger is the region of observers in the shadow zone. The optimal engine positions take advantage of that in order to maximize noise shielding. The optimal engine positions considering creeping rays are slightly upstream compared with the optimal positions determined for a sharp leading edge: 0.5 m for the inboard engines and 2 m for the outboard engines. This is in agreement with experimental results of noise shielding for a NACA 0012 airfoil [27,28]. These experiments showed that a noise source located at the airfoil leading edge presented higher values of shielding than when located at the trailing edge.

In the following sections, the aircraft design has been adapted to these most promising engine locations, and an overall noise assessment is presented along an approach and a departure trajectory.

2. *Departure: Trajectory, Emission, and Noise Impact*

The departure trajectory of the $B744_{rr}$ and the $B744_{eow}$ aircraft is presented in Fig. 11. The two trajectories show small differences due to the better performance of the $B744_{rr}$, because the $B744_{eow}$ presents increased weight due to the larger wing and higher fuel consumption.

The aircraft noise emission, 12.5 km after departure, is shown in Fig. 12 ($h = 800$ m, $v = 130$ m/s, no high lift devices, $N_1 = 100\%$). The engine positions and the noise shielding values differ considering a sharp or curved leading edge. This results in noise emissions as shown in Figs. 12a and 12b.

The total noise level of the reference aircraft, $B744_{rr}$, is represented by the dashed dotted line. The black line represents the noise emission of the $B744_{eow}$, considering a sharp (Fig. 12a) and a curved (Fig. 12b) leading edge. The difference between the solid and the dashed black lines is larger in Fig. 12a, i.e., considering a sharp leading edge. The forward and aft fan noise are also represented in the plots, showing that the forward fan noise is more shielded for the sharp leading edge and the aft fan noise is more shielded for the curved leading edge. Because of the fan noise reduction, jet and airframe noise have an important contribution to the total noise of the $B744_{eow}$, contrary to the case of the $B744_{rr}$, in which fan noise was clearly dominant (see Fig. 8b).

The SEL contour areas are used to assess the ground noise impact: Fig. 13 shows the SEL values of the $B744_{eow}$ in relation to the $B744_{rr}$; i.e., negative values mean that the $B744_{eow}$ has lower SEL than the $B744_{rr}$. Again, the sharp and curved leading-edge cases are analyzed separately in Figs. 13a and 13b, respectively.

The predicted noise reduction is higher considering a sharp leading edge than for a curved leading edge, for a large area of the contour. The difference becomes noticeable about 7 km downrange of brake release, where the engine speed is reduced to cutback rotational speed; thus the jet noise is reduced, and fan noise dominates. The red dots in the plots are related with the higher MTOW of the $B744_{eow}$, which implies a longer takeoff distance.

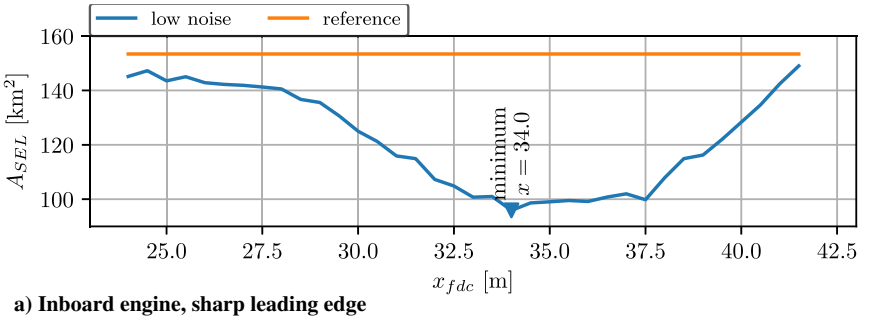

a) Inboard engine, sharp leading edge

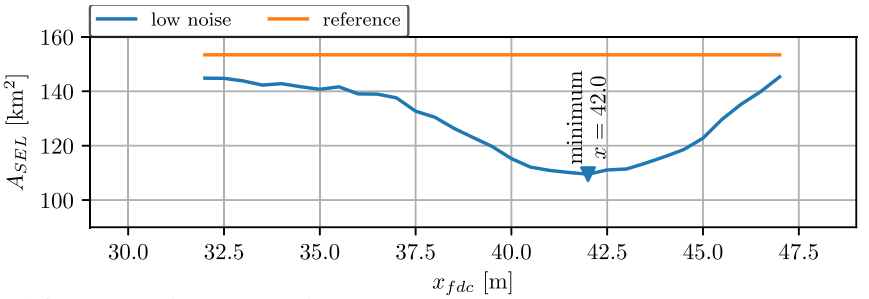

b) Outboard engine, sharp leading edge

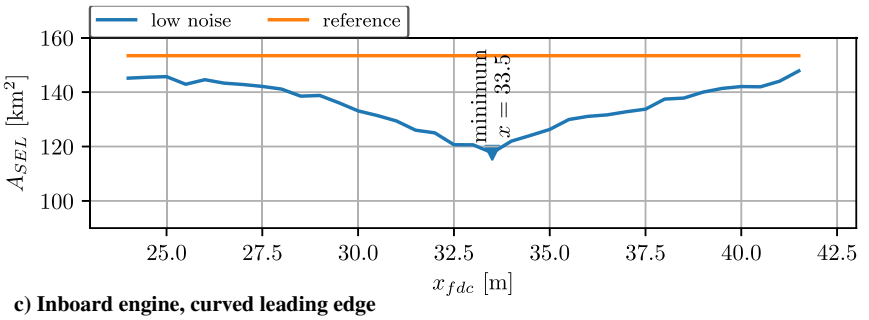

c) Inboard engine, curved leading edge

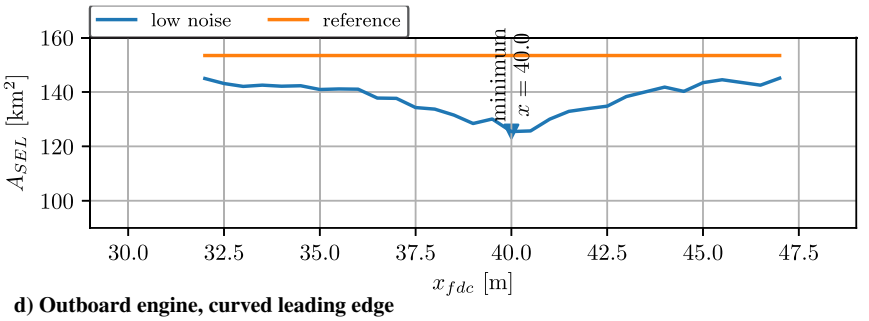

d) Outboard engine, curved leading edge

Fig. 9 SEL isocontour area of 80 dB plotted versus x_{fdc}, for departure.

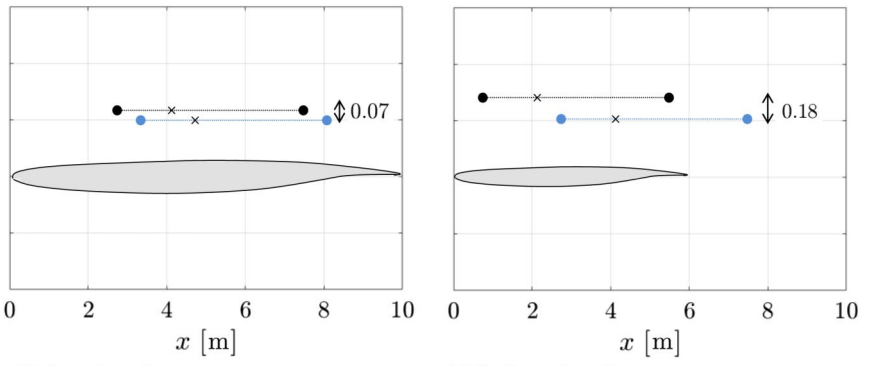

a) Inboard engine **b) Outboard engine**

Fig. 10 Position of the inboard and outboard engines in the chord. The engine inlet and exhaust positions are indicated in blue and black, for the sharp and curved leading-edge approximations, respectively.

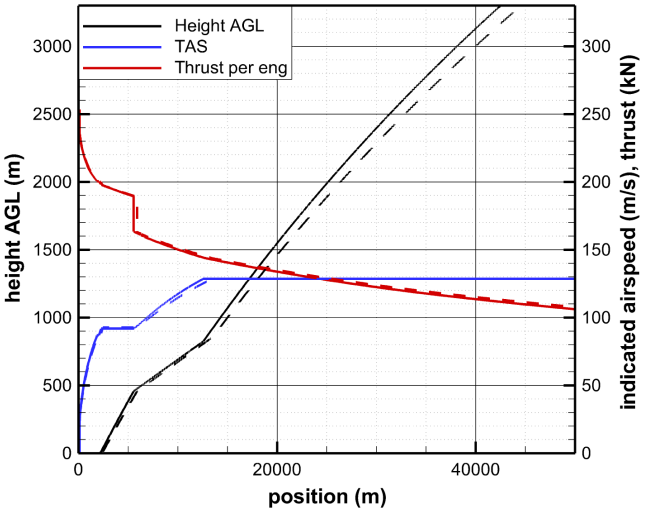

Fig. 11 Low-noise departure trajectories for the $B744_{rr}$ (solid lines) and the $B744_{eow}$ (dashed lines).

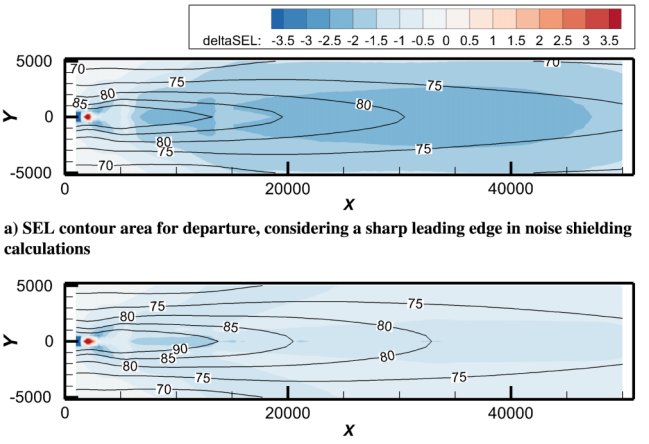

a) SEL contour area for departure, considering a sharp leading edge in noise shielding calculations

b) SEL contour area for departure, considering a curved leading edge in noise shielding calculations

Fig. 13 SEL values for departure of the $B744_{rr}$ (lines), and ΔSEL values of the $B744_{eow}$ relative to the $B744_{rr}$ (color).

3. *Approach: Trajectory, Emission, and Noise Impact*

The low-noise approach trajectories of the $B744_{rr}$ and the $B744_{eow}$ are illustrated in Fig. 14. As for the case of the departure, the two trajectories are very similar and the slight differences are attributed to the increased wing area of the $B744_{eow}$.

Figure 15 shows the aircraft noise level at 15 km before approach threshold ($h = 800$ m, $v = 98$ m/s, $N_1 = 35\%$.). At this position flaps are set to 15° and the Kruger flaps are set. The aircraft decelerates for landing, and therefore the engines are still in idle. The overall noise is therefore dominated by airframe noise, and the difference between the solid and the dashed black lines in Figs. 15a and 15b is the same. The slight noise reduction of the $B744_{eow}$ compared with the $B744_{rr}$ is due to the lower flight speed, not noise shielding.

Figure 16 shows the impact on ground of the $B744_{eow}$ relative to the $B744_{rr}$. Again, both the sharp and curved leading-edge cases are considered: the overall noise emission is very similar because of the little impact of fan noise and, consequently, of the shielding effect.

Away from touchdown, the engine is idle and the SEL reduction is attributed to the decrease in airspeed along the $B744_{eow}$ trajectory.

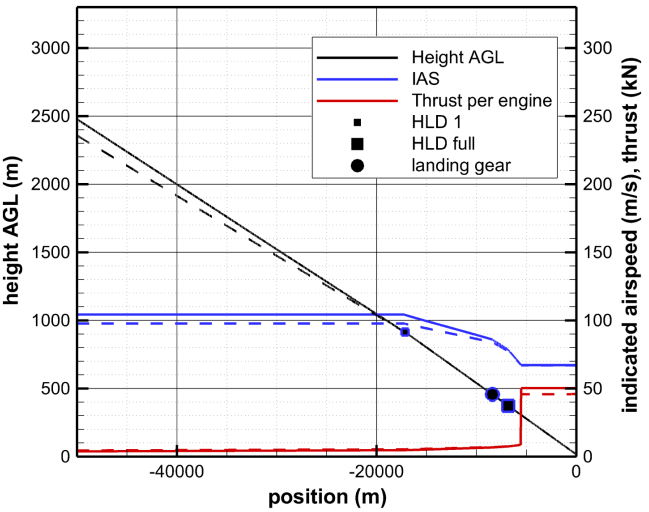

Fig. 14 Low-noise approach trajectory for the $B744_{rr}$ (solid lines) and the $B744_{eow}$ (dashed lines).

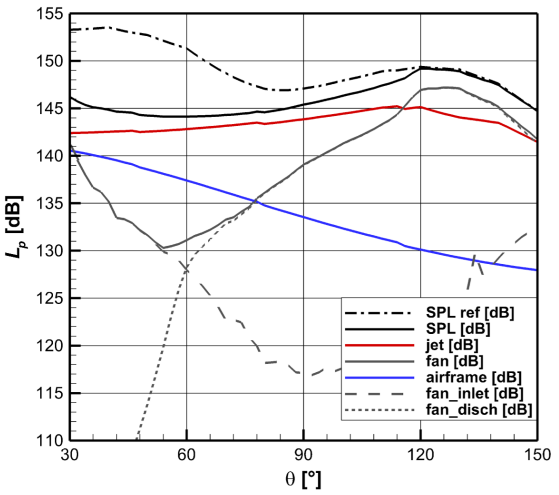

a) Noise emission of the $B744_{eow}$ calculated with a sharp leading edge

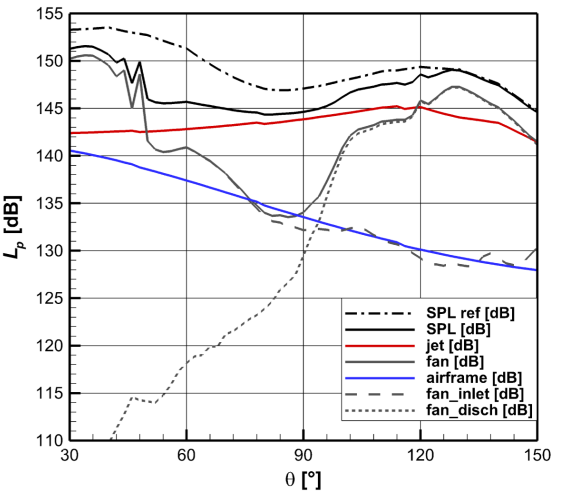

b) Noise emission of the $B744_{eow}$ calculated with a curved leading edge

Fig. 12 Overall sound emission of the $B744_{eow}$ for the departure condition selected.

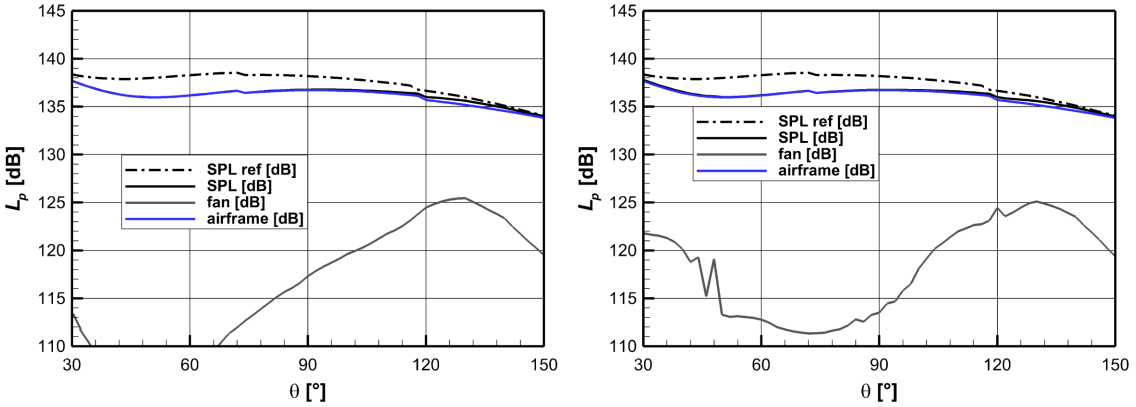

a) Noise emission of the B744$_{eow}$ calculated with a sharp leading edge

b) Noise emission of the B744$_{eow}$ calculated with a curved leading edge

Fig. 15 Overall sound level of the *B*744$_{eow}$ for the approach condition selected.

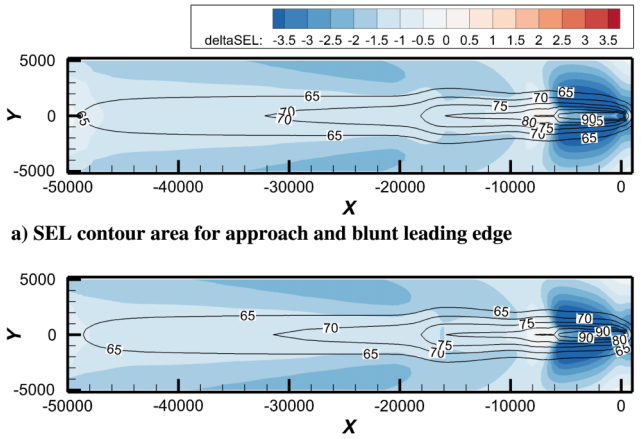

a) SEL contour area for approach and blunt leading edge

b) SEL contour area for approach and creeping ray around leading edge

Fig. 16 SEL values for approach of the *B*744$_{rr}$ (lines), and Δ SEL values of the *B*744$_{eow}$ relative to the *B*744$_{rr}$ (color).

After the deployment of the landing gear, at approximately 6 km before touchdown the engines are spooled up to compensate the drag, and the fan noise becomes significant compared with airframe noise, originating higher reduction of SEL in both Figs. 16a and 16b.

V. Conclusions

Different levels of details to simulate fan noise shielding can be implemented, i.e., accounting for creeping rays or simplification of the problem via sharp edges. A simulation tool of TU Delft allows to implement both methods and to directly assess the resulting differences. To transfer these differences to the aircraft system noise level, the shielding results are furthermore processed in a low-noise aircraft design process. Therefore, a dedicated application example was selected from an ongoing DLR research project. A B747-400 variant with over-the-wing engines, denominated *B*744$_{eow}$, was selected in order to reduce the ground noise impact through shielding of the engine noise. In a first step, the most promising engine location for maximum shielding was determined. The resulting vehicles are then subjected to a dedicated ground noise analysis including an approach and departure situation. The analysis considered the changes in aerodynamics and flight performance of the modified aircraft, which resulted in modifications of the geometry (wing area, aspect ratio, and sweep) and operational conditions (lower cruise speed and higher fuel consumption) compared with the original aircraft.

Moving the engines from their original position under the wing affected the aerodynamics of the vehicle, and therefore the payload range chart. The top-level aircraft requirements had to be adjusted to obtain a realizable aircraft and flight profile. Low-noise approach and departure trajectories were obtained, and the noise impact on ground was estimated. The optimal positions of inboard and outboard engines for the *B*744$_{eow}$ were determined based on SEL contour area during departure, as it is the flight phase in which the fan is the most significant noise source.

The optimal position for the inboard engine considering a sharp leading edge is close to the case of a curved leading edge, with a difference of 0.5 m (equal to the discretization step). However, for the outboard engines the positions differ by 2 m. The optimal engine positions considering a curved leading edge are moved upstream in the chord direction in comparison with the sharp leading-edge approximation. In addition, the fan disk center is approximately centered in the chord in order to maximize the number of receiver positions in the deep shadow zone. This is in agreement with experimental data found in the literature for the variation of noise shielding for different source positions on the chord of a NACA 0012 airfoil. However, it is important to mention that the case of fan noise, analyzed in this work, is more complex, with an inlet and exhaust contributions.

For departure, fan noise is reduced considering both a sharp and curved leading edge, but with lower values for the latter. Jet noise, which was noticeably lower than fan noise for the *B*744$_{rr}$, plays an important role in the total noise of the *B*744$_{eow}$. The SEL contours show a maximum reduction of 2 dB considering a sharp leading edge and of 1.5 dB for the curved leading edge for the *B*744$_{eow}$ compared with the *B*744$_{rr}$.

The same analysis was performed for approach. In this case, airframe noise dominates and the shielding of fan noise is relevant only at the final phase of approach, when the engines are spooled up to compensate the drag. However, there is a slight decrease of SEL for the *B*744$_{eow}$ during the entire trajectory, which is due to the reduced airspeed of the trajectory.

In conclusion, it was verified that deviations in the optimal engine positions and in the noise reduction predictions can occur if the curvature of the leading edge is not accounted for. However, the engines in this aircraft are positioned very close to a large wing, which presents a significant influence of the creeping rays compared with smaller conventional aircraft. This emphasizes the importance of the creeping rays for this particular design. It is recommended based on the findings of this study to account for creeping rays when dealing with large wing areas. Rough geometry approximations in the noise shielding predictions can influence the optimal location of the engines on a large wing. For small wing areas or aft-mounted engines, the influence of the creeping rays is expected to be small (as observed for the Fokker 70 in the validation section).

Appendix A: B747-400 Payload Range Chart

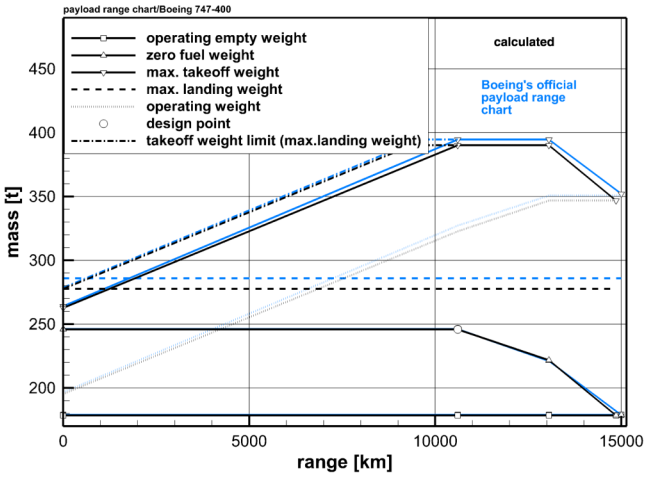

Fig. A1 Predicted payload range chart compared and Boeing's official data [29].

Appendix B: Characteristics of the $B744_{rr}$ and $B744_{eow}$

Design	A_{wing}, m^2	λ_F	MTOW, ton	M_{cruise}	Cruise fuel, ton	$E_{cruise,beg}$	Λ, °
$B744_{rr}$	562	7.18	350	0.85	108	17.5	38.6
$B744_{eow}$	580	8.00	369	0.70	125	17.0	38.9

References

[1] "Concept of a Balanced Approach Principle to Aircraft Noise Management, Appendix C of Assembly Resolution A35," International Civil Aviation Organization (ICAO) Air Transport Bureau (ATB), 2007, http://www.icao.int/env/noise.htm [retrieved 21 April 2018].

[2] "Erste Verordnung zur Durchfuehrung des Gesetzes zum Schutz gegen Fluglaerm (Verordnung ueber die Datenerfassung und das Berechnungsverfahren für die Festsetzung von Laermschutzbereichen–1. FlugLSV)," Bundesgesetzblatt BGBl I, Bundesministerium der Justiz, 2008.

[3] Thomas, J., and Hansman, R., "Framework for Analyzing Aircraft Community Noise Impacts of Advanced Operational Flight Procedures," *Journal of Aircraft*, Vol. 56, No. 4, 2019, pp. 1–11. https://doi.org/10.2514/1.C035100

[4] Bertsch, L., "*Noise Prediction Within Conceptual Aircraft Design*," Deutsches Zentrum für Luft-und Raumfahrt (DLR) TR DLR-FB-2013-20, Göttingen, 2013.

[5] Bertsch, L., Wolters, F., Heinze, W., Pott-Pollenske, M., and Blinstrub, J., "System Noise Assessment of a Tube-and-Wing Aircraft with Geared Turbofan Engines," *Journal of Aircraft*, Vol. 56, No. 4, 2019, pp. 1577–1596. https://doi.org/10.2514/1.C034935

[6] Filippone, A., and Bertsch, L., "Comparison of Aircraft Noise Models with Flyover Data," *Journal of Aircraft*, Vol. 51, No. 3, 2014, pp. 1043–1046. https://doi.org/10.2514/1.C032368

[7] Filippone, A., Zhang, M., and Bojdo, N., "Validation of an Integrated Simulation Model for Aircraft Noise and Engine Emissions," *Aerospace Science and Technology*, Vol. 89, June 2019, pp. 370–381. https://doi.org/10.1016/j.ast.2019.04.008

[8] Vieira, A., Snellen, M., and Simons, D., "Assessing the Shielding of Engine Noise by the Wings for Current Aircraft Using Model Predictions and Measurements," *Journal of the Acoustical Society of America*, Vol. 143, No. 1, 2018, pp. 388–398. https://doi.org/10.1121/1.5020798

[9] Vieira, A., Malgoezar, A., Snellen, M., and Simons, D., "Analysis of Shielding of Propeller Noise Using Beamforming and Predictions," *Journal of the Acoustical Society of America*, Vol. 146, No. 2, 2019, pp. 1085–1098. https://doi.org/10.1121/1.5121398

[10] Bertsch, L., Dobrzynski, W., and Guérin, S., "Tool Development for Low-Noise Aircraft Design," *Journal of Aircraft*, Vol. 47, No. 2, 2012, pp. 694–699. https://doi.org/10.2514/1.43188

[11] Bertsch, L., Schäffer, B., and Guérin, S., "Uncertainty Analysis for Parametric Aircraft System Noise Prediction," *Journal of Aircraft*, Vol. 56, No. 2, 2018, pp. 529–544. https://doi.org/10.2514/1.C034809

[12] Heinze, W., "*Ein Beitrag zur quantitativen Analyse der Technischen und Wirtschaftlichen Auslegungsgrenzen verschiedener Flugzeugkonzepte für den Transport Grosser Nutzlasten*," ZLR Forschungsbericht TR 94-01, Braunschweig, 1994.

[13] Becker, R., Wolters, F., Nauroz, M., and Otten, T., "Development of a Gas Turbine Performance Code and Its Application to Preliminary Engine Design," DLRK 2011, Deutscher Luft- und Raumfahrtkongress, Bremen, Germany, 2011.

[14] Blinstrub, J., "*Immission-Based Noise Reduction Within Conceptual Aircraft Design*," Deutsches Zentrum für Luft-und Raumfahrt (DLR) TR DLR-FB-2019-12, Göttingen, 2019.

[15] Blinstrub, J., Bertsch, L., and Heinze, L., "Assessment of the Noise Immission Along Approach and Departure Flightpaths for Different SFB880 Vehicle Concepts," *24th AIAA/CEAS Aeroacoustics Conference*, AIAA Paper 2018-2818, 2018. https://doi.org/10.2514/6.2018-2818

[16] Bertsch, L., "Noise Prediction Toolbox Used by the DLR Aircraft Noise Working Group," Inter-Noise 2013, 2013.

[17] Koch, M., and Bertsch, L., "Engine Noise Source Placement for Shielding Calculation," Inter-Noise 2019, 2019.

[18] Rego, L., Avallone, F., Ragni, D., and Casalino, D., "Jet-Installation Noise and Near-Field Characteristics of Jet–Surface Interaction," *Journal of Fluid Mechanics*, Vol. 895, July 2020, p. A2. https://doi.org/10.1017/jfm.2020.294

[19] Keller, J., "Geometrical Theory of Diffraction," *Journal of the Optical Society of America*, Vol. 52, No. 2, 1962, pp. 116–130. https://doi.org/10.1364/JOSA.52.000116

[20] Schultheisz, C., "Numerical Solution of the Huygens–Fresnel–Kirchhoff Diffraction of Spherical Waves by a Circular Aperture," *Journal of the Optical Society of America*, Vol. 11, No. 2, 1994, p. 774–778. https://doi.org/10.1364/JOSAA.11.000774

[21] Umul, Y., "Modified Diffraction Theory of Kirchhoff," *Journal of the Optical Society of America*, Vol. 25, No. 8, 2008, pp. 1850–1860. https://doi.org/10.1364/JOSAA.25.001850

[22] Jiménez, J., and Hita, E., "Babinet's Principle in Scalar Theory of Diffraction," *Optical Review*, Vol. 8, No. 6, 2001, p. 495. https://doi.org/10.1007/BF0293174

[23] Heinze, W., Oesterheld, C., and Horst, P., "Multidisziplinaeres Flugzeugentwurfsverfahren PrADO–Programmentwurf und Anwendung im Rahmen von Flugzeugkonzeptstudien," Jahrbuch der DGLR-Jahrestagung 2001, 2001.

[24] Werner-Westphal, W., Heinze, W., and Horst, P., "Multidisciplinary Integrated Preliminary Design Applied to Unconventional Aircraft Configurations," *Journal of Aircraft*, Vol. 45, No. 2, 2008, pp. 581–589. https://doi.org/10.2514/1.32138

[25] Wolters, F., and Becker, R., "Engine Performance Simulation of the Integrated V2527-Engine Fan," *54th AIAA Aerospace Sciences Meeting*, AIAA Paper 2016-0388, 2016. https://doi.org/10.2514/6.2016-0388

[26] Smith, M., *Aircraft Noise*, Cambridge Univ. Press, New York, 1989.

[27] Hutcheson, F., Bahr, C., and Thomas, R., "Experimental Study of Noise Shielding by a NACA 0012 Airfoil," *2018 AIAA/CEAS Aeroacoustics Conference*, AIAA Paper 2018-2821, 2018. https://doi.org/10.2514/6.2018-2821

[28] Rossignol, K., and Delfs, J., "Analysis of the Noise Shielding Characteristics of a NACA0012 2D Wing," *22nd AIAA/CEAS Aeroacoustics Conference*, AIAA Paper 2016-2795, 2006. https://doi.org/10.2514/6.2016-2795

[29] "747-400 Airplane Characteristics for Airport Planning, D6-58326-1, Manual," Boeing Commercial Airplanes, Seattle, WA, 2002.